# FUSION OF MULTIPLE LOW-RESOLUTION NASA AIRBORNE SNOW OBSERVATORY (ASO) LIDAR DATA FOR FOREST VEGETATION STRUCTURE CARACTERIZATION

*Antonio Ferraz[1], Sassan Saatchi [1], Kat J. Bormann [1], Thomas H. Painter[1]*

1- Jet Propulsion Laboratory, California Institute of Technology, Pasadena, CA, USA

## ABSTRACT

Airborne lidar provides timely updated maps for monitoring forest change at high resolution but it has been little used for that purpose due to the scarcity of long-term time-series over a common area. The NASA Jet Propulsion Laboratory Airborne Snow Observatory (ASO) is a landscape-level monitoring system that provides ongoing multi-year remote sensing measurements over mountainous ecosystems to primary quantify snow volume and dynamics. It collects low-resolution lidar data (~1.5 pt/m$^2$) with a nominal weekly frequency up to 12 times a year with measurements that span 2013-2017 over 12 mountain watersheds across the western US that currently face ecological threads.

In this work, we present a method to automatically register ASO weekly low-resolution lidar point clouds in order to calculate spatially consistent datasets (~12 pt/m$^2$) adapted to fine scale forestry studies. We test the method using 12 lidar datasets acquired over the Tuolumne River Basin (Sierra Nevada, California) in the spring and summer of 2014. On average, the ASO lidar system provides accurate measurements in terms of geolocation (0.38m and 0.12m for the horizontal and vertical dimension, respectively) but some datasets are biased up to 1.38m and 0.53m, respectively. Our registration method successfully corrected for systematic bias improving the 3D geometry of forest point clouds.

***Index Terms***— lidar, time series, point cloud registration, forest structures analysis

## 1. INTRODUCTION

There is a lack of time series maps to understand forest disturbance and regeneration processes over the forests in the Sierra Nevada (California) forests that are currently experiencing dramatic tree mortality rates due to severe insect and drought damage [1], [2]. More than 102 million trees died in California forests and the state government as being in greatest need of tree removal because they represent potential direct threat to people and infrastructures from falling trees as well as boarder fire risk and forest health. Timely updated maps of dead tree and corresponding volume would help forest managers in optimizing resources and reduce costs. Field inventory approaches are constrained by the spatial and temporal frequency of sampling and hence might not adequately capture disturbance and regeneration processes. The current time-series of maps to characterize forest dynamics have been computed using multispectral and radar imagery that are not suited to study many ecological processes in detail (e.g. fuel bed loads accumulation, tree recruitment) because they are not able to characterize 3D forest structure.

Airborne lidar provides spatially explicit maps of forest 3D structure at the landscape level that are increasingly needed by the scientific community to support a wide range of activities [3], [4]. However, the availability of forest 3D maps has been limited by the high cost associated with acquiring lidar data with the resolution required to properly characterize forest horizontal and vertical structure (>8 pts/m$^2$). Most forestry studies have been based on a snapshot and there is no long-term time-series of data to investigate forest dynamics.

The NASA-JPL Airborne Snow Observatory (ASO) offers a unique opportunity to study Californian forests dynamics at the landscape level. It offers multiple acquisitions over mountain systems each winter and spring in, at present, 12 mountain watersheds (Figure 1a) that are populated by vegetated areas of ecological interest over the Sierra Nevada (California, since 2013), The Rocky Mountains (Colorado, since 2013), Mount Jefferson (Oregon, since 2016), and Mount Olympus (Washington, since 2014). The ASO is a scanning lidar system coupled to an imaging spectrometer which main purpose is to monitor spatial distribution of snow volume and dynamics over mountains watersheds ([5]). To do this, ASO weekly over-flights mountainous areas several times a year during snowfall and snowmelt seasons. In addition, there is an additional flight in snow-off conditions to calculate the corresponding Digital Terrain Models (DTM), which is combined with snow-on products to estimate the snow depth for a given date. However, the point density of the weekly measurements (~1.5 pts/m$^2$) is not adapted to analyze forest structure in detail (e.g. forest vertical structure, individual tree crowns, fuel bed loads). In this work, we coherently fusion the low-density weekly ASO measurements to calculate a high-density density point cloud to properly characterize vegetation structure in detail.

We developed a new method to register the ASO low-resolution time series of lidar data. Former methods are not adapted to the ASO data because they have been developed

to apply to high-density point clouds mainly over urban areas where the identification of corresponding points (which are commonly called tie points and are crucial to align point clouds) can be achieved thought the extraction of easily recognized features (e.g. roads intersections, roofs edges). However, the low resolution of our datasets as well as the dynamics of our landscape introduced by snow and ice events makes the identification of such features difficult.

## 2. MATERIAL

### 2.1. Study site

Our study site is located in the Tuolumne River Basin on the west side of the Sierra Nevada, California (Figure 1, [6]). The Tuolumne Basin above the O'Shaughnessy Dam has ~1100 km$^2$ area, of which ~40% is covered by forests of California red fir, Jeffrey pine and Douglas fir. Elevations range from 1190 m at the dam up to 4000 m at the summit of Mt Lyell, the highest point in Yosemite National Park at the southern end of the basin. We selected a study site with significant vegetation cover (7 km x 4 km rectangle in Figure 1a)

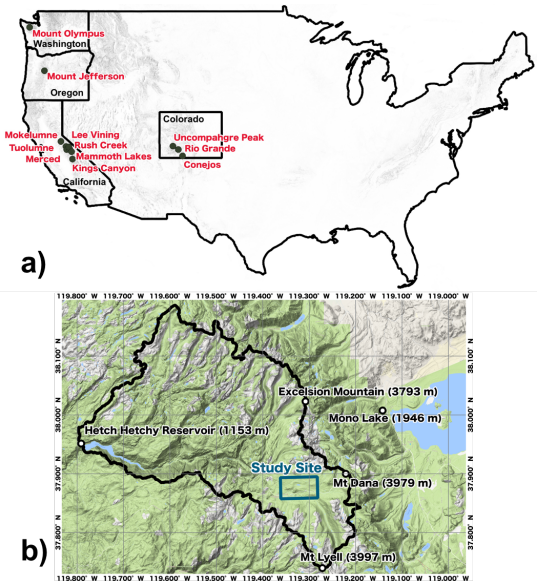


**Figure 1.** Airborne Snow Observatory (ASO) coverage sites (**a**, black dots) across the US and a **b)** zoom over the Tuolumne River basin study site (, blue rectangle, 7 km x 4 km) in the Sierra Nevada, California Well know locations are provided for better location.

### 2.2. Lidar data

The study site was measured in twelve different dates in 2014 using the ASO Riegl Q1560 scanning lidar system in full-waveform mode. Eleven of twelve datasets were acquired in snowon conditions between March 23$^{rd}$ and June 5$^{th}$ whereas the remaining summer acquisition (August 27$^{th}$) mapped the ground topography. The position and orientation of the platform are given by onboard GPS/IMU measurements. In addition, the onboard GPS measurements are calibrated using differential position correction using GPS base stations. The expected final point density for the weekly acquisitions is of 1.5 pts/m$^2$. The ground points have been classified using the TerraScan software [7]. Note that, in snowon conditions the points classified as ground may correspond to the snow surface.

## 3. METHODS

The first step consists in removing the lidar points corresponding to the snow surface from the snowon acquisitions. Otherwise, they would be confused with low vegetation because they show higher altitude regarding the bare ground topography. To do this, we simple remove all the points lower than 30 cm from a surface computed using the points classified as ground. In the second step, we apply the new registration method developed to apply for low-density lidar point clouds over natural landscapes. The latter is based in a coordinates transformation model defined by:

$$\begin{pmatrix} x_a^{i,j} \\ y_a^{i,j} \\ z_a^{i,j} \end{pmatrix} = \begin{pmatrix} \Delta x^j \\ \Delta y^j \\ \Delta z^j \end{pmatrix} + R^j(\alpha,\beta,\gamma) \begin{pmatrix} x_o^{i,j} \\ y_o^{i,j} \\ z_o^{ii,j} \end{pmatrix} \quad (1)$$

Where $X_o^{i,j} = (x_o^{i,j}, y_o^{i,j}, z_o^{i,j})$ and $X_a^{i,j} = (x_a^{i,j}, y_a^{i,j}, z_a^{i,j})$ are the coordinates of the original and adjusted lidar point clouds, respectively; $i = 1, \dots n$ and $j = 1, \dots, m$ where $n$ is the number of points in a given point cloud and $m$ the number of lidar acquisitions; $V^j = (\Delta x^j, \Delta y^j, \Delta z^j)$ is a translation vector and $R^j(\alpha,\beta,\gamma)$ a 3D rotation matrix defined by the axis angles $(\alpha,\beta,\gamma)$. To solve Eq. 1) in order to calculate the corresponding translation vector and rotation matrix for each weekly acquisition, we define a datasets of tie objects that need to have at least four elements because Eq. 1) is defined in three dimensions. To play the role of tie objects, we manually select isolated tree apexes because they are the landscape feature that changes the less with snowfall and ice events. However, the identification of the tree apexes on the weekly acquisitions is difficult due to the fact that most likely the lidar misses the tree apex because of the low spatial resolution of the measurements. We decided to select the nearest lidar point from each weekly acquisition as the best proxy for the tie object location (called vertices, Figure 2a). Then, we adjust the location of each tie objects by calculating the barycenter of the multiple vertices (Figure 2b). Finally, we calculate a transformation model for each lidar acquisition. To do this, we set the coordinates of the vertices, $X_o^{i,j}$, for each acquisition in Eq. 1). The corresponding translation vector $V^j$ and transformation matrix $R^j$ give us the magnitude and direction of the geolocation error for a given acquisition. To visually assess such errors, we normalize the coordinates of the vertices using the coordinates of the corresponding tie objects. It

allows computing a scatterplot where the coordinates of the vertices correspond to the distance and direction to the corresponding tie object (Figure 2c). The spatial distribution of the vertices with respect to the origin of the scatter plot is a good indicator of the nature and magnitude of the geolocation errors. For instance, if their majority is located towards a given direction, it means that there is a systematic location error. The modes of the vertices locations allow to visually identify systematic bias (larger dots in Figure 2c).

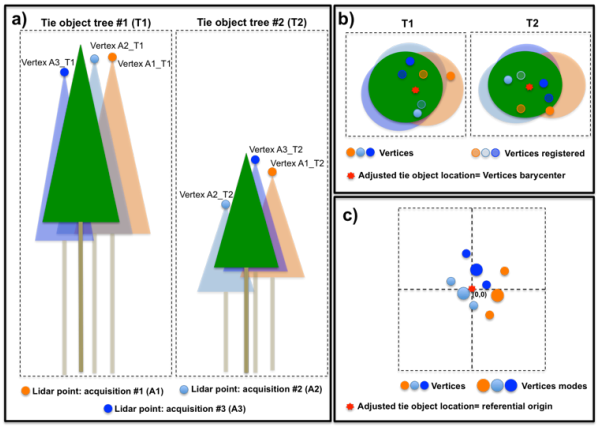


**Figure 2.** Registration method scheme with **a)** two isolated trees selected as tie objects (green trees T1 and T2) and the highest neighbor lidar points from the weekly acquisitions (called vertices). **b)** The location of the tie objects is adjusted to the vertices barycenter (red asterisk). In **c)**, the coordinates of the vertices have been normalized using the corresponding tie object location for visualization purposes. The larger dots correspond to the mode of the vertices and are a good estimator for the magnitude and direction of the geolocation errors for each weekly acquisition.

## 4. RESULTS AND DISCUSSION

Results are assessed over the study site shown in Figure 1. For this study, we defined twenty tie objects distributed over the area of interest by identifying isolated trees (green dots in Figure 1). Figure 3a shows the weekly acquisitions merged before our registration method is applied. In general, the point clouds are spatially consistent but some acquisitions (e.g. March 2014) show a large location bias regarding the remaining ones that jeopardizes the forest features outlines (e.g. tree apexes).

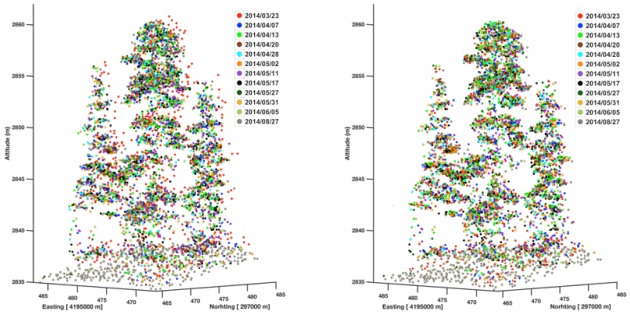

**Figure 3.** Point cloud merged **a)** before and **b)** after registration.

Figure 4a shows the coordinates of the vertices normalized by the coordinates of the corresponding tie objects as explained in Figure 2c. A similar analysis is made for the altitude of the points (Figure 4b). Therefore, the locations of the modes of the vertices (represented by the larger dots) are a good indicator for the magnitude and direction of the misalignment between acquisitions. The acquisitions of March the 23rd, and May the 11th, they both show a significant systematic geolocation error in planimetric dimension, whereas only the former acquisition has important issues in altimetry. Figure 4c and d show the scatter plots after applying our method. As expected, the modes of the individual acquisitions overlap in the origin of the graphs, whereas the spread of the vertices changed little with respect to the original data. Indeed, the purpose of our method was not to adjust individually the vertices because they might not correspond exactly to the location of the tie objects due to the low resolution of the data. The goal was to find a global solution able to remove systematic geolocation errors. The goal was achieved because the modes they all overlap to the origin (Figure 4c and d).

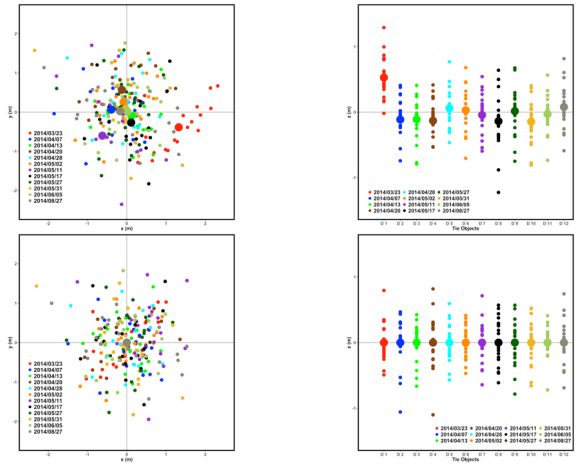

**Figure 4.** Vertices grouped by acquisition date (small dots) and corresponding modes (large dots) in the horizontal (figures in the left) and vertical (figures in the right) dimensions. Top and bottom images correspond to the analysis before and after registration, respectively.

Figure 5 shows the magnitude of the registration vector for each weekly acquisition calculated using the translation vector $V^j$ and transformation matrix $R^j$ (Eq. 1). At some extent, Figure 5 quantifies the errors show by the larger dots in Figure 4a and b. With respect to the horizontal dimension, most of the datasets show very low bias. The only two exceptions have a moderate strong and a moderate bias slightly higher than 1.3m and 0.8m, respectively. As far as the vertical domain is concerned, most of the measurements are quite accurate (~0.2m) with a single exception (~ *0.52m*). Results show that the geolocation error of the ASO system is larger in the horizontal dimension than in the

vertical one. The results of the point cloud adjustments are show in Figure 3b, which compares to Figure 3a after applying our registration method. It means that our method succeeded in removing the bias visible in the original measurements. For instance, the comparison between the figures shows that the bias of the point cloud acquired in March the 23rd of 2014 has been corrected and now better matches the remaining datasets.

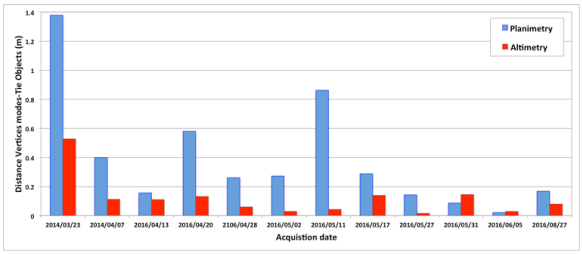


**Figure 5.** Size of the registration vector for the weekly acquisitions calculated from the coordinates transformation models (Eq. 1).

Finally, Figure 6 shows a single acquisition dataset and the high-density point cloud calculated by merging the co-registered individual acquisitions. The latter represents the forest structure at a finer resolution in both horizontal and vertical dimensions and enables the lidar forest inventory at the individual tree level, which is crucial for the monitoring of tree mortality as well as for tree biomass estimates over areas with inexistent field sampling [8], [9].

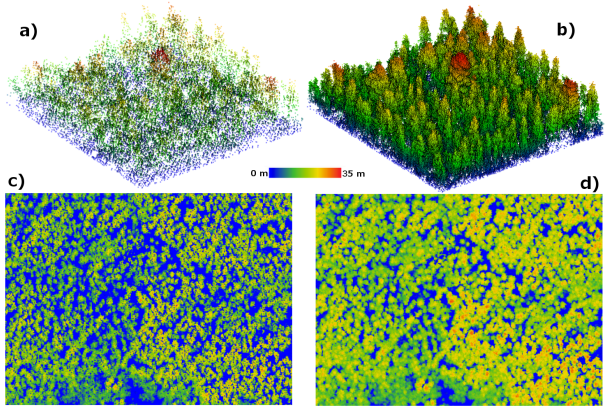


**Figure 6.** Point cloud (100m x 100m) calculated using **a)** a low-density single acquisition and **b)** a high-resolution multi-temporal point cloud after co-registration. The canopy height models (1m resolution, 350m x 250 m) have been calculated using a single **(c)** and twelve **(d)** lidar acquisitions.

## 5. CONCLUSION

We concluded that ASO lidar time-series have the potential to characterize forest structure at a fine scale. Although the nominal flights of the ASO for snowpack monitoring provide lower resolution datasets with limited capabilities for vegetation sampling, its high temporal resolution enables the calculation of high-resolution point clouds by merging individual acquisitions. First, we examined the ASO lidar system reliability in terms of geolocation because it directly impacts the consistency of the high-density product. The tests were carried out using 12 lidar acquisitions over the Tuolumne River basin. Our point cloud registration method shows very satisfactory results in compensating for erroneous GPS/IMU measurements. Important improvements have been done regarding the main features of the forest (e.g. tree apexes) indicating that our method improves the spatial consistency of the high-density point cloud by correcting for both large and small systematic bias.

The ASO offers a unique high-resolution lidar dataset to monitor forest change over ecosystems with high impact on many ecological and hydrological processes. It is a unique opportunity to study the impact of intense drought and warming climate change on forest disturbance and regrowth, tree recruitment and mortality, and fuel load accumulation.

## ACKNOWLEDGMENTS

The research was carried out at the Jet Propulsion Laboratory, California Institute of Technology, under a contract with the National Aeronautics and Space Administration.

## REFERENCES

[1] G. P. Asner, P. G. Brodrick, C. B. Anderson, N. Vaughn, D. E. Knapp, and R. E. Martin, "Progressive forest canopy water loss during the 2012–2015 California drought," *Proc. Natl. Acad. Sci.*, vol. 2015, p. 201523397, 2015.

[2] M. Meyer, B. Bulaon, M. MacKenzie, and H. Safford, "Mortality, structure, and regeneration in whitebark pine stands impacted by mountain pine beetle in the southern Sierra Nevada," *Can. J. For. Res.*, vol. 46, no. 4, pp. 572–581, Jan. 2016.

[3] M. A. Wulder *et al.*, "Lidar sampling for large-area forest characterization: A review," *Remote Sens. Environ.*, vol. 121, pp. 196–209, 2012.

[4] S. G. Zolkos, S. J. Goetz, and R. Dubayah, "A meta-analysis of terrestrial aboveground biomass estimation using lidar remote sensing," *Remote Sens. Environ.*, vol. 128, pp. 289–298, 2013.

[5] T. H. Painter *et al.*, "The Airborne Snow Observatory: Fusion of scanning lidar, imaging spectrometer, and physically-based modeling for mapping snow water equivalent and snow albedo," *Remote Sens. Environ.*, vol. 184, pp. 139–152, Oct. 2016.

[6] A. Ferraz, S. Saatchi, K. J. Bormann, and T. H. Painter, "Fusion of NASA Airborne Snow Observatory (ASO) Lidar Time Series over Mountain Forest Landscapes," *Remote Sens.*, vol. 10, no. 2, 2018.

[7] A. Soininen, "TerraScan User's guide. Available online at: http://www.terrasolid.com/guides/tscan/index.html (accessed: 28/01/2017)." 2011.

[8] A. Ferraz, S. Saatchi, C. Mallet, and V. Meyer, "Lidar detection of individual tree size in tropical forests," *Remote Sens. Environ.*, vol. 183, pp. 318–333, 2016.

[9] D. a. Coomes and R. B. Allen, "Mortality and tree-size distributions in natural mixed-age forests," *J. Ecol.*, vol. 95, no. 1, pp. 27–40, 2007.